Since January 2020 Elsevier has created a COVID-19 resource centre with free information in English and Mandarin on the novel coronavirus COVID-19. The COVID-19 resource centre is hosted on Elsevier Connect, the company's public news and information website.

Available online at www.sciencedirect.com
ScienceDirect
Biochemical and Biophysical Research Communications 369 (2008) 344–349
BBRC
www.elsevier.com/locate/ybbrc

Lipid rafts are involved in SARS-CoV entry into Vero E6 cells

Yanning Lu [a,d], Ding Xiang Liu [a,b], James P. Tam [a,c,*]

[a] School of Biological Sciences, Nanyang Technological University, 60 Nanyang Drive, Singapore 637551, Singapore
[b] Institute of Molecular and Cell Biology, 61 Biopolis Drive, Proteos, Singapore 138673, Singapore
[c] The Scripps Research Institute, 5353 Parkside Drive, Jupiter, FL 33458, USA
[d] Beijing Center for Diseases Prevention and Control, 16 Hepingli Middle Street, Dongcheng District, Beijing 100013, China

Received 15 January 2008
Available online 13 February 2008

Abstract

Lipid rafts often serve as an entry site for certain viruses. Here, we report that lipid rafts in Vero E6 cells are involved in the entry of severe acute respiratory syndrome coronavirus (SARS-CoV). Infectivity assay showed the integrity of lipid rafts was required for productive infection of pseudotyped SARS-CoV. Depletion of plasma membrane cholesterol with MβCD relocalized raft-resident marker caveolin-1 as well as SARS-CoV receptor ACE2 to a nonraft environment, but did not significantly change the surface expression of ACE2. MβCD-treatment inhibited infectivity of pseudotyped SARS-CoV by 90%. Biochemical fractionation and confocal imaging confirmed that ACE2 colocalized with raft-resident markers. Furthermore, an ectodomain of SARS-CoV S protein (S1188HA) could associate with lipid rafts after binding to its receptor, and colocalize with raft-resident marker ganglioside GM1. The binding of S1188HA was not affected by depleting plasma membrane cholesterol. Taken together, our results support that lipid rafts serve as an entry port for SARS-CoV.

Keywords: Lipid rafts; SARS-CoV; Vero E6; ACE2; Spike protein; Entry

Lipid rafts are functional membrane microdomains rich in cholesterol and sphingolipids. They serve as domains to concentrate membrane-associated proteins that include receptors and signaling molecules [1]. In polarized cells, lipid rafts are concentrated at the apical surface whereas, in nonpolarized cells, they are dispersed over the cell surface [2].

In addition to the demonstrated physiological roles in signal transduction of host cells [1,3], lipid rafts often serve as a site for entry, assembly and budding of microbial pathogens [4–6]. Recent studies have implicated lipid rafts in the entry process of HIV-1 [7], simian virus 40 [8]. There was also some evidence that lipid rafts are involved in coronavirus entry. In the case of human coronavirus 229E (HCoV-229E), virus entry was inhibited by depletion of cholesterol, resulting in the disruption of viral association with the cellular receptor, CD13 [9]. Thorp and Gallagher [10] showed that lipid rafts were crucial for the entry of MHV. SARS-CoV is a novel coronavirus discovered in association with cases of severe acute respiratory syndrome (SARS) in 2003. Although the detailed mechanism remains to be determined, the early step in the entry process of SARS-CoV into target cells is initiated by engagement of its cellular receptor, angiotensin-converting enzyme 2 (ACE2), by the spike (S) glycoprotein [11]. The African green monkey kidney cell, Vero E6 cell, is a cell line that permits replication of SARS-CoV. It provides a useful reagent to examine the yet undetermined roles of lipid rafts in SARS-CoV entry process. Here, we report that SARS-CoV receptor ACE2 is localized in lipid rafts in Vero E6 cells and the productive entry of SARS-CoV pseudovirus into Vero E6 cells requires the presence of intact lipid rafts.

* Corresponding author. Address: The Scripps Research Institute, 5353 Parkside Drive, Jupiter, FL 33458, USA. Fax: +1 561 799 8568.
E-mail address: jamestam@scripps.edu (J.P. Tam).

0006-291X/$ - see front matter © 2008 Published by Elsevier Inc.
doi:10.1016/j.bbrc.2008.02.023

Materials and methods

Reagents. Paraformaldehyde, bovine serum albumin (BSA) and methyl-β-cyclodextrin (MβCD) were purchased from Sigma. Alexa 594 conjugates of CT-B, Alexa 488 conjugates of donkey anti-goat, anti-mouse, and anti-rabbit antibodies, rabbit anti-CT-B and the ProLong antifade kit were purchased from Molecular Probes. Mouse anti-HA (F-7), rabbit anti-HA (Y-11), and rabbit anti-caveolin-1 (N-20) antibodies were purchased from Santa Cruz Biotechnology, goat anti-ACE2 (AF933) antibody was purchased from R&D systems, mouse anti-CD71 antibody was purchased from Zymed Laboratories Inc. HRP-conjugated rabbit anti-mouse and anti-goat antibodies, swine anti-rabbit antibody were purchased from DakoCytomation.

Cell cultures. Vero E6 and 293T cells were maintained in DMEM with 10% new born calf serum and 50 μg/ml penicillin–streptomycin (Gibco). Sf9 cells were maintained in Sf-900 II SFM (Gibco).

Expression and purification of SARS-CoV S protein ectodomain. The nucleotide fragment corresponding to 1–1188 amino acid residues of SARS-CoV S protein were amplified with a HA tag at the C-terminus (S1188HA). Primers used were A (5′-AGTCGAATTCCGAAC ATGTTT ATTTTCTTA-3′) and B (5′-GCCCTCTAGATTAAGCGTAATCTGGA ACATCGTA TGGGTACATCTCGAGATATTTTCCCAATTCTT-3′). The fragment was inserted into the transfer vector pVL1392 (BD Bioscience Pharmingen). The resulted plasmid was co-transfected with linearized baculovirus DNA (BD Biosciences) into Sf9 cells. Successful recombinant baculoviruses were selected and amplified. Sf9 cells were infected with the recombinant baculovirus at a multiplicity of infection (moi) of 3–10. At 4 days post-infection, cells were collected and lysed in lysis buffer (50 mM Tris, pH 7.5; 150 mM NaCl; 0.1% Nonidet P40; complete protease inhibitor cocktail). The protein was purified using the anti-HA affinity column (Roche applied Science).

Preparation of pseudotyped SARS-CoV. The pseudovirus was generated by co-transfection of pNL4-3Luc$^+$Env$^-$Vpr$^-$ and pcDNA3.1-OPT9-S or pVPack-VSV-G (Stratagene) into 293T cells using calcium phosphate transfection method. The culture supernatant containing virus was collected on day 2 and 3 after transfection and clarified by filtering it through a 0.45 μm-pore-size filter and concentrated. The virus titer was determined by the reverse transcriptase (RT) activity assay using EnzChek® reverse transcriptase assay kit (Molecular Probes).

Single-cycle infectivity assay. Vero E6 cells (30,000 cells/well) were seeded in 48-well plates and cultured at 37 °C 5% CO_2 overnight. On the following day, Vero E6 cells (untreated or treated with 10 mM MβCD) were incubated with standardized amounts of pseudoviruses (0.5 U of RT/well) for 1 h and washed. After 48 h of infection, the cells were lysed in 100 μl lysis buffer (Promega). Luciferase activity was determined using luciferase assay kit (Promega). The resultant scintillation was counted for 15 s using a TD-20/20 Luminometer (Tuner Designs).

Cholesterol depletion. The cells were washed twice with DMEM and then incubated with 10 mM MβCD in DMEM-0.1% BSA for 30 min at 37 °C. Under these conditions, cell viability was not significantly affected, as determined by trypan blue exclusion. As controls, the cells were exposed to medium alone at 37 °C. After incubation, the cells were washed twice with ice-cold DMEM-0.1% BSA before being used.

Membrane flotation analysis. Cells (5×10^7) were washed twice with ice-cold PBS and lysed on ice for 30 min in 1 ml TNE buffer (25 mM Tris [pH 7.5], 150 mM NaCl, 5 mM EDTA, complete protease inhibitor cocktail) with 1% Triton X-100. The cell lysates were homogenized by a Dounce homogenizer, and then centrifuged for 5 min, 720*g* at 4 °C to remove insoluble materials and nuclei. The supernatant was mixed with 1 ml 80% sucrose in TNE buffer, placed at the bottoms of ultracentrifuge tubes, overlaid with 6 ml 30% and 3 ml 5% sucrose in TNE buffer. The cell lysates were ultracentrifuged at 4 °C for 18 h at 38,000 rpm in a SW41 rotor (Beckman). After centrifugation, eleven 1-ml fractions were collected from the top to the bottom and analyzed immediately by Western blot or stored at −80 °C. To investigate the presence of S protein ectodomain in lipid rafts after binding to its receptor, Vero E6 cells were incubated with S1188HA (10 μg/ml) for 30 min at 4 °C, after extensive washing with PBS, the cells were lysed and lipid rafts were isolated.

About 20 μl of individual sucrose gradient fractions were resolved by 8% or 15% SDS–PAGE gels. The proteins were transferred to PVDF membranes and probed with primary antibody: rabbit anti-caveolin-1, mouse anti-CD71 and goat anti-ACE2 or rabbit anti-HA antibodies, then following with secondary antibody: HRP-conjugated swine anti-rabbit, rabbit anti-mouse and rabbit anti-goat antibodies as described previously. Bound antibodies were detected with the ECL Plus Western blotting detection reagents (Amersham Biosciences).

Flow cytometry. Expression of ACE2 on the surface of Vero E6 cells and the binding of S1188HA to Vero E6 cells were evaluated by flow cytometry. Untreated or MβCD-treated cells were collected and incubated for 30 min at 4 °C with or without S1188HA (10 μg/ml), after washing three times with PBS, the cells were incubated with goat anti-ACE2 antibody or rabbit anti-HA antibody. The cells were washed three times with PBS and incubated with Alexa 488-conjugated donkey anti-goat or donkey anti-rabbit antibody for 30 min at room temperature. After washing, samples were analyzed on a Becton Dickinson FACSCalibur within 2 h of immunofluorescence staining.

Raft aggregation and confocal microscopy. To investigate the presence of ACE2 in lipid rafts, Vero E6 cells were first incubated with Alexa 594-conjugated CT-B (10 μg/ml) and goat anti-ACE2 antibodies at 4 °C for 30 min in PBS with 0.1% BSA, followed by extensive washing with ice-cold PBS. To investigate the presence of S protein ectodomain in lipid rafts after binding to its receptor, Vero E6 cells were incubated with S1188HA (10 μg/ml) at 4 °C for 30 min, then the cells were labeled with Alexa 594-conjugated CT-B and mouse anti-HA antibodies. Lipid rafts aggregation was initiated by incubation with rabbit anti-CT-B in the presence of Alexa 488-conjugated donkey anti-goat antibody or Alexa 488-conjugated donkey anti-mouse antibody at 4 °C for 30 min. After washing twice with ice-cold PBS, the cells were fixed at 4 °C for 15 min with fresh 4% paraformaldehyde. In addition, lipid rafts ganglioside GM1 was identified by incubation with Alexa 594-conjugated CT-B alone. The cells were washed, fixed, and mounted with a ProLong antifade kit. Labeled cells were analyzed by a Zeiss LSM 510 META confocal microscope using 100× objective lenses. The images were processed by LSM 510 META software.

Results

ACE2 is localized in lipid rafts in Vero E6 cells, cholesterol depletion does not affect the surface expression of ACE2, but shifted it to nonraft fraction

ACE2 was identified as a functional receptor for SARS-CoV [11]. We determined its relationship with lipid rafts by biochemical fractionation and confocal microscopy. In normal Vero E6 cells, approximately 70% of ACE2 was co-fractionated with the raft marker caveolin-1 in fractions 3 and 4 (Fig. 1A, untreated). In contrast, a nonraft marker, transferrin receptor CD71 [12], was confined to the detergent-soluble fractions 10 and 11 (Fig. 1A, untreated). The results show that ACE2 is largely associated with lipid rafts in Vero E6 cells.

After extraction of cholesterol, the localization of CD71 in cellular membrane remained unchanged (Fig. 1A, MβCD-treated), but both ACE2 and caveolin-1 were shifted to fractions 10 and 11 (Fig. 1A, MβCD-treated). No obvious change in the cell surface expression of ACE2 was observed (Fig. 1C) using flow cytometry. The results indicate that disruption of lipid rafts does not block the translocation of ACE2 to the cell surface.

The association of ACE2 with lipid rafts was investigated in intact cells by confocal microscopy. The fluores-

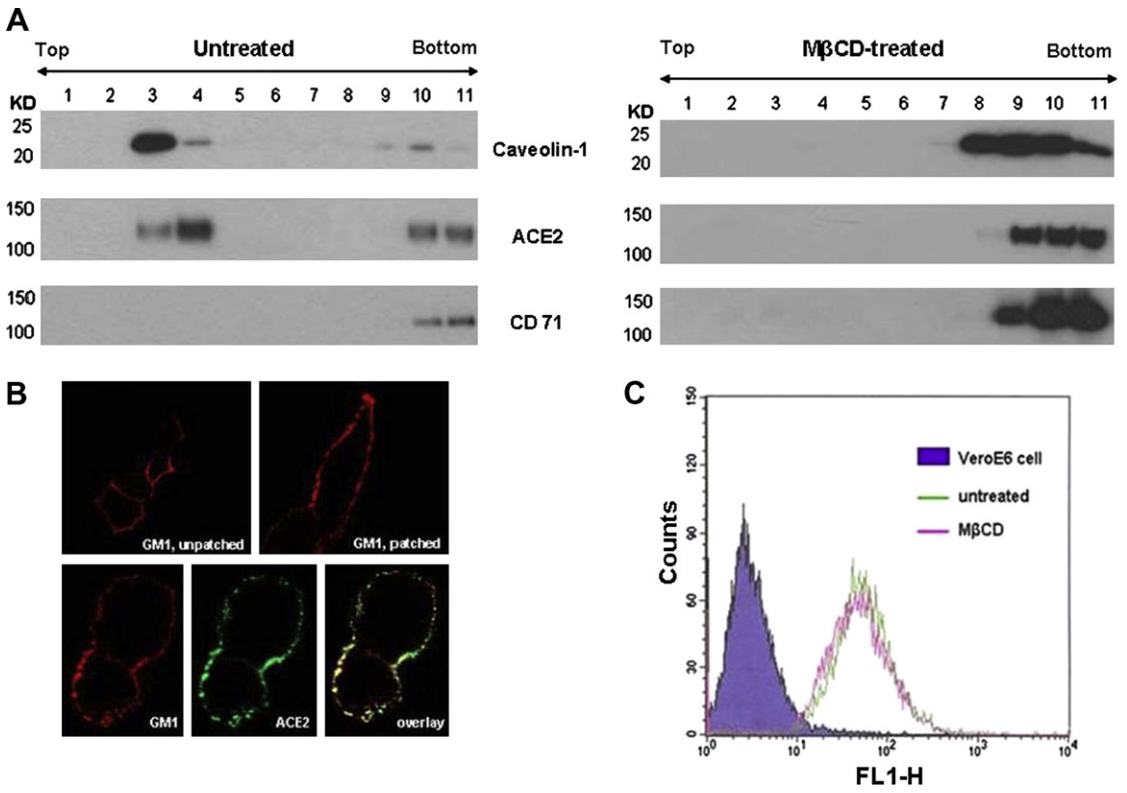

Fig. 1. Localization of ACE2 in lipid rafts in untreated or MβCD-treated Vero E6 cells. (A) Sucrose gradient fractionation. ACE2, caveolin-1, and CD71 in individual fractions were detected separately by Western blot. (B) Confocal microscopy. Single confocal sections are shown. Colocalization of ACE2 and GM1 (B, overlay). Cells incubated with Alexa 594-conjugated CT-B alone show uniform distribution of GM1 (B, GM1, unpatched). While incubation with anti-CT-B antibody led to formation of large GM1 patches (B, GM1, patched). (C) Flow cytometry. The solid peak in blue was detected from the Vero E6 cells without antibody labeling to serve as the blank of this experiment. (For interpretation of the references to color in this figure legend, the reader is referred to the web version of this article.)

cently labeled CT-B could specifically binds to a raft-resident ganglioside GM1 [12]. Treatment of Vero E6 cells with Alexa 594-conjugated CT-B alone resulted in a uniform unpatched staining pattern of the plasma membrane (Fig. 1B, GM1, unpatched). However, incubation with rabbit anti-CT-B led to the formation of large GM1 patches (Fig. 1B, GM1, patched). Incubation of cells simultaneously with Alexa 594-conjugated CT-B/rabbit anti-CT-B and goat anti-ACE2/Alexa 488-conjugated donkey anti-goat antibody, resulted in substantial colocalization of ACE2 with GM1 patches (Fig. 1B overlay). The results demonstrate that ACE2 and GM1 reside in the same lipid environment in Vero E6 cells.

An ectodomain of SARS-CoV S protein is associated with lipid rafts in Vero E6 cells upon binding to its receptor

Since ACE2 was shown to be present in lipid rafts, we next investigated the relationship of SARS-CoV S protein with rafts after binding to Vero E6 cells. For this purpose, we prepared an ectodomain (S1188HA) of S protein (aa 1–1188) with a HA tag at the C-terminus (Fig. 2A). The protein was expressed in Sf9 cells and purified to near homogeneity (Fig. 2B, lane 3). The results show that the majority of S1188HA was co-fractionated with caveolin-1 after binding to its receptor (Fig. 2C, fractions 3 and 4). A minor proportion of the protein was also detected in soluble fractions (Fig. 2C, fraction 11). The association of S1188HA with lipid rafts was further investigated in intact cells by confocal microscopy. The results suggest that the S1188HA colocalized with GM1 (Fig. 2D, overlay).

Depletion of cholesterol does not affect the binding of SARS-CoV S protein ectodomain to Vero E6 cell

The effect of cholesterol depletion on the binding of S1188HA to Vero E6 cells was investigated by biochemical fractionation. In contrast to the results obtained from untreated cells, depletion of cholesterol resulted in the detection of S1188HA in the soluble fractions as well as caveolin-1 (Fig. 3A).

S1188HA binding to MβCD-treated Vero E6 cells was further analyzed by flow cytometry. No obvious shifting of peaks was observed, indicating that S1188HA bound equally well to MβCD-treated or untreated Vero E6 cells (Fig. 3B). In agreement with the biochemical data, these results show that the ectodomain of S protein could efficiently bind to Vero E6 cells regardless of the integrity of lipid rafts.

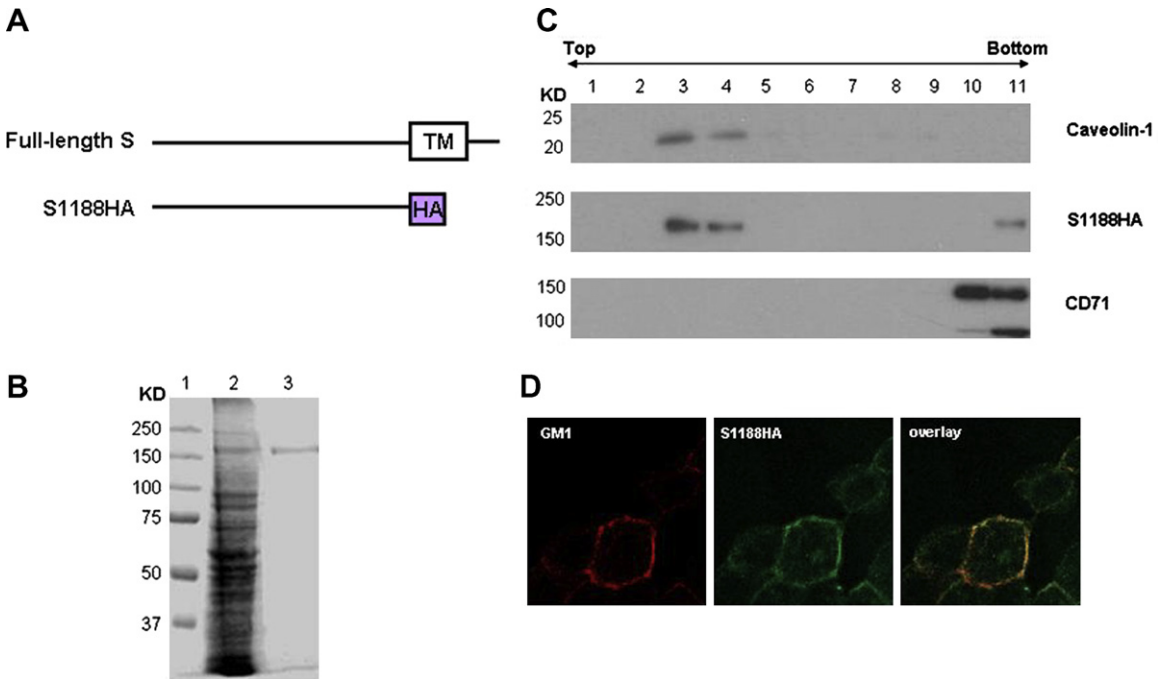

Fig. 2. Association of S1188HA with lipid rafts in Vero E6 cells. (A) Schematic representations of S protein and S1188HA (aa 1–1188). (B) SDS–PAGE analysis of SH1188HA. The cell lysate (lane 1) and affinity-purified protein (lane 2) were stained with Coomassie blue R250. (C) Cofraction of caveolin-1 and S1188HA were detected in each fraction by Western blot. (D) Confocal microscopy to show colocalization of GM1 and S1188HA (overlay).

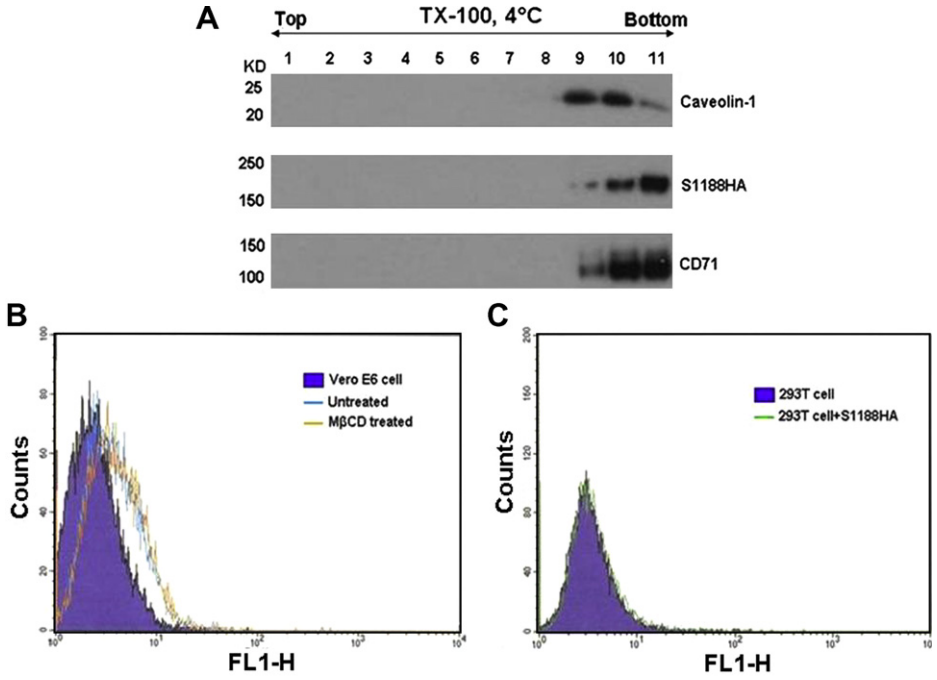

Fig. 3. Effects of cholesterol depletion on the association of S1188HA with lipid rafts. (A) Sucrose gradient analysis. Caveolin-1, S1188HA and CD71 were detected by Western blot. (B and C) Flow cytometry analysis. Peak shift was observed in the Vero E6 cells incubated with S1188HA comparing with the negative control (solid-Vero E6 cell labeled with primary and secondary antibody, without S1188HA incubation). No peak shift was observed in untreated and MβCD-treated Vero E6 cells , and 293T cells incubated with or without S1188HA.

Depletion of cholesterol inhibits productive infectivity of pseudotyped SARS-CoV in Vero E6 cells

The effect of cholesterol depletion on the entry of SARS-CoV into Vero E6 cells was investigated using a single-cycle infectivity assay. Virions pseudotyped with SARS-CoV S protein or with the envelope glycoprotein G of VSV (VSV-G) were used to infect untreated (control) or MβCD-treated Vero E6 cells. Negligible background level of luciferase activity could be detected in lysates prepared

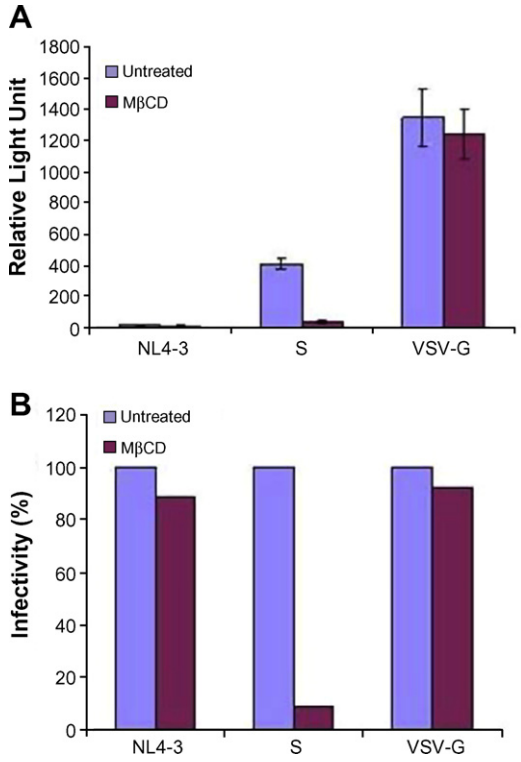

Fig. 4. Effects of cholesterol depletion on the infectivity of pseudotyped SARS-CoV. Untreated (control) or MβCD-treated Vero E6 cells were infected with pNL4-3Luc^{+}Env^{-}Vpr^{-} virions, (NL4-3) or SARS-CoV or VSV-G pseudoviruses. (A) Luciferase activity in 20 μl of cell lysates (expressed as relative light units) was determined using luciferase assay reagent. (B) The infectivity of untreated cell of each group served as 100% infectivity, the infectivity (%) of MβCD-treated cell of each group was calculated based on their own negative control (untreated cell). The results are representative of three independent experiments.

from the cells infected with pNL4-3Luc^{+}Env^{-}Vpr^{-} virions (Fig. 4, NL4-3). Productive infection of SARS-CoV pseudovirus was inhibited about 90% after depletion of cholesterol (Fig. 4, S), but the infectivity of VSV pseudovirus did not change significantly (Fig. 4, VSV-G). These results demonstrate that disruption of lipid rafts dramatically inhibits productive infection of viruses pseudotyped with SARS-CoV S protein but not VSV-G, which enter the cell through a rafts-independent pathway [13].

Discussion

Entry of SARS-CoV into permissive cells, like other coronaviruses, is mediated through the binding of its S protein to cellular receptor [14]. Thus, the differential expression of its receptor, ACE2 [15] could contribute to the entry process of SARS-CoV. ACE2 is abundantly expressed on the surface of lung and intestinal epithelial cells, consistent with their susceptibility to SARS-CoV [16]. Additionally, epithelial cells are highly polarized cells, and ACE2 is expressed predominately on the apical surface of these cells [17] where lipid rafts are concentrated. Although it has been shown that lipid rafts are important for the entry of coronaviruses, such as HCoV-229E [9] and MHV [10], its role in SARS-CoV entry is undetermined.

Several aspects of the entry mechanism of SARS-CoV were clarified recently. Simmons et al. [18,19] have provided strong evidence to show that SARS-CoV enters cell by an endosomal pathway, and the cleavage of S protein to S1 and S2 by cathepsin L is necessary for fusion. Matsuyama et al. [20] found that various proteases, such as trypsin are effective in inducing fusion of SARS-CoV-infected Vero E6 cells. So SARS-CoV has the potential to enter host cells via two different pathways, either an endosomal or a non-endosomal pathway, depending on the presence of proteases. In either of these pathways, only S protein bound to its receptor and cleaved by proteases could obtain fusion activity. The distribution of its receptors plays important roles in its entry.

In this study, lipid rafts were shown to be engaged in the entry process of SARS-CoV into Vero E6 cells. We demonstrated that ACE2 was largely colocalized with raft marker caveolin-1 and GM1. Our results are different from the results of Turner's group [17]. They found that ACE2 is not raft-localized in CHO Cells. By now whether the raft localization of ACE2 is cell type specific has not been confirmed yet. Our results show that ACE2 was shifted to the nonraft environment after depletion of cholesterol. Using single-cycle infectivity assay, we also found that depletion of cholesterol from cell membranes resulted in 90% reduction of the luciferase activity in cells infected with SARS-CoV pseudovirus but not VSV pseudovirus. Furthermore, the cell surface expression of ACE2 and the binding of S protein ectodomain to Vero E6 cells did not change significantly after cholesterol depletion. The results eliminate the possibility that MβCD inhibits viral entry by down regulating the receptor, and subsequently deceasing the virus binding. All the evidence suggests that raft integrity is crucial for productive entry of SARS-CoV pseudovirus into Vero E6 cells and specific concentration of ACE2 in lipid rafts may explain why SARS-CoV selects these microdomains for entry. The preferential association of an ectodomain of S protein with lipid rafts further supports our hypothesis that SARS-CoV receptor localizes in these microdomains and represents the population of membrane receptor engaged in virus binding and entry.

How does lipid rafts affect the efficiency of SARS-CoV entry and productive infection? Coronaviruses enter the host cells either by direct membrane fusion with the plasma membrane or by receptor-mediated endocytosis. Membrane fusion is a cooperative process, and lipid rafts concentrate components of the membrane docking and fusion machinery for endocytosis [21], such as actin polymerization [22] which is important for the membrane fusion and endocytosis. An increased concentration of these proteins in rafts facilitates their intermolecular interactions by proximity. Nicolau et al. [23] used a stochastic spatial model of the plasma membrane to investigate the role of lipid rafts in signal transduction. Their results showed that partitioning of protein into rafts increases

specific interprotein collision rates. Thus, rafts serve as membrane "reaction vessels", increasing the chance for two specific proteins of low concentration to meet on the membrane and in turn, increasing the collision rate to increase the efficiency of membrane reactions. In the case of SARS-CoV, lipid rafts could provide a convenient platform to concentrate receptor ACE2 as clusters on host cell membrane to dock efficiently with the spike protein on viral envelope. The finding that CD209 L (L-SIGN), a C-type lection-associated with lipid rafts serving as an alternative receptor for SARS-CoV [24], lends further support to our view. Induced by virus binding, lipid rafts are aggregated as a reaction platform by the stimulation of signaling pathways emanating from these microdomains to facilitate the sequential incorporation and fusion process.

In conclusion, we present data demonstrating the essential role of lipid raft in Vero E6 cells to support productive viral infection. Understanding of the entry mechanism could lead to the development of effective anti-SARS-CoV drug therapies that interfere with ACE2 receptor localization in rafts and rafts-mediated entry.

Acknowledgment

We thank Prof. Zhang Linqi (Aaron Diamond AIDS Research Center, Rockefeller University, New York, NY 10016) for providing plasmids: pNL4-3Luc^{+}Env^{-}Vpr^{-} and pcDNA3.1-OPT9-S.

References

[1] K. Simons, E. Ikonen, Functional rafts in cell membranes, Nature 387 (6633) (1997) 569–572.
[2] A. Pralle, P. Keller, E.L. Florin, K. Simons, J.K. Horber, Sphingolipid–cholesterol rafts diffuse as small entities in the plasma membrane of mammalian cells, J. Cell Biol. 148 (5) (2000) 997–1008.
[3] K. Simons, D. Toomre, Lipid rafts and signal transduction, Nat. Rev. Mol. Cell Biol. 1 (1) (2000) 31–39.
[4] O. Kovbasnjuk, M. Edidin, M. Donowitz, Role of lipid rafts in Shiga toxin 1 interaction with the apical surface of Caco-2 cells, J. Cell Sci. 114 (Pt. 22) (2001) 4025–4031.
[5] S.S. Rawat, M. Viard, S.A. Gallo, A. Rein, R. Blumenthal, A. Puri, Modulation of entry of enveloped viruses by cholesterol and sphingolipids (review), Mol. Membr. Biol. 20 (3) (2003) 243–254.
[6] M. Suomalainen, Lipid rafts and assembly of enveloped viruses, Traffic 3 (10) (2002) 705–709.
[7] W. Popik, M.A. Timothy, W.-C. Au, Human Immunodeficiency virus type 1 uses lipid rafts-colocalized CD4 and chemokine receptors for productive entry into CD4+ T cells, J. Virol. 76 (10) (2002) 4709–4722.
[8] L. Pelkmans, J. Kartenbeck, A. Helenius, Caveolar endocytosis of simian virus 40 reveals a new two-step vesicular-transport pathway to the ER, Nat. Cell Biol. 3 (5) (2001) 473–483.
[9] R. Nomura, A. Kiyota, E. Suzaki, K. Kataoka, Y. Ohe, K. Miyamoto, T. Senda, T. Fujimoto, Human coronavirus 229E binds to CD13 in rafts and enters the cell through caveolae, J. Virol. 78 (16) (2004) 8701–8708.
[10] E.B. Thorp, T.M. Gallagher, Requirements for CEACAMs and cholesterol during murine coronavirus cell entry, J. Virol. 78 (6) (2004) 2682–2692.
[11] W. Li, M.J. Moore, N. Vasilieva, J. Sui, S.K. Wong, M.A. Berne, M. Somasundaran, J.L. Sullivan, K. Luzuriaga, T.C. Greenough, H. Choe, M. Farzan, Angiotensin-converting enzyme 2 is a functional receptor for the SARS coronavirus, Nature 426 (6965) (2003) 450–454.
[12] P.W. Janes, S.C. Ley, A.I. Magee, Aggregation of lipid rafts accompanies signaling via the T cell antigen receptor, J. Cell Biol. 147 (2) (1999) 447–461.
[13] C. Aiken, Pseudotyping human immunodeficiency virus type 1 (HIV-1) by the glycoprotein of vesicular stomatitis virus targets HIV-1 entry to an endocytic pathway and suppresses both the requirement for Nef and the sensitivity to cyclosporin A, J. Virol. 71 (8) (1997) 5871–5877.
[14] H. Hofmann, S. Pohlmann, Cellular entry of the SARS coronavirus, Trends Microbiol. 12 (10) (2004) 466–472.
[15] C.T. Tseng, J. Tseng, L. Perrone, M. Worthy, V. Popov, C.J. Peters, Apical entry and release of severe acute respiratory syndrome-associated coronavirus in polarized Calu-3 lung epithelial cells, J. Virol. 79 (15) (2005) 9470–9479.
[16] I. Hamming, W. Timens, M.L. Bulthuis, A.T. Lely, G.J. Navis, H. van Goor, Tissue distribution of ACE2 protein, the functional receptor for SARS coronavirus. A first step in understanding SARS pathogenesis, J. Pathol. 203 (2) (2004) 631–637.
[17] F.J. Warner, R.A. Lew, A.I. Smith, D.W. Lambert, N.M. Hooper, A.J. Turner, Angiotensin-converting enzyme 2 (ACE2), but not ACE, is preferentially localized to the apical surface of polarized kidney cells, J. Biol. Chem. 280 (47) (2005) 39353–39362.
[18] G. Simmons, J.D. Reeves, A.J. Rennekamp, S.M. Amberg, A.J. Piefer, P. Bates, Characterization of severe acute respiratory syndrome-associated coronavirus (SARS-CoV) spike glycoprotein-mediated viral entry, Proc. Natl. Acad. Sci. USA 101 (12) (2004) 4240–4245.
[19] G. Simmons, D.N. Gosalia, A.J. Rennekamp, J.D. Reeves, S.L. Diamond, P. Bates, Inhibitors of cathepsin L prevent severe acute respiratory syndrome coronavirus entry, Proc. Natl. Acad. Sci. USA 102 (33) (2005) 11876–11881.
[20] S. Matsuyama, M. Ujike, S. Morikawa, M. Tashiro, F. Taguchi, Protease-mediated enhancement of severe acute respiratory syndrome coronavirus infection, Proc. Natl. Acad. Sci. USA 102 (35) (2005) 12543–12547.
[21] T. Lang, D. Bruns, D. Wenzel, D. Riedel, P. Holroyd, C. Thiele, R. Jahn, SNAREs are concentrated in cholesterol-dependent clusters that define docking and fusion sites for exocytosis, Embo. J. 20 (9) (2001) 2202–2213.
[22] P. Caroni, New EMBO members' review: actin cytoskeleton regulation through modulation of PI(4,5)P(2) rafts, Embo. J. 20 (16) (2001) 4332–4336.
[23] D.V. Nicolau Jr., K. Burrage, R.G. Parton, J.F. Hancock, Identifying optimal lipid raft characteristics required to promote nanoscale protein–protein interactions on the plasma membrane, Mol. Cell Biol. 26 (1) (2006) 313–323.
[24] S.A. Jeffers, S.M. Tusell, L. Gillim-Ross, E.M. Hemmila, J.E. Achenbach, G.J. Babcock, W.D. Thomas Jr., L.B. Thackray, M.D. Young, R.J. Mason, D.M. Ambrosino, D.E. Wentworth, J.C. Demartini, K.V. Holmes, CD209L (L-SIGN) is a receptor for severe acute respiratory syndrome coronavirus, Proc. Natl. Acad. Sci. USA 101 (44) (2004) 15748–15753.